






Local viscoelastic properties and shear stress propagation in bulk and confined polymer melts and low-molecular weight liquids

Alireza F. Behbahani ^{1,2,*}, Petra Bačová ^{2,3,†}, Patrycja Polińska⁴, Craig Burkhart ⁵,
Manolis Doxastakis ⁶ and Vagelis Harmandaris ^{2,7,8,‡}

¹Institut für Physik, Johannes Gutenberg-Universität Mainz, Staudingerweg 7, D-55099 Mainz, Germany

²Institute of Applied and Computational Mathematics, Foundation for Research and Technology - Hellas, Heraklion GR-71110, Greece

³Departamento de Ciencia de los Materiales e Ingeniería Metalúrgica y Química Inorgánica, Facultad de Ciencias, IMEYMAT, Campus Universitario Río San Pedro s/n., Puerto Real, Cádiz 11510, Spain

⁴Goodyear S.A., Avenue Gordon Smith, Colmar-Berg L-7750, Luxembourg

⁵The Goodyear Tire & Rubber Company, 142 Goodyear Boulevard, Akron, Ohio 44305, USA

⁶Department of Chemical and Biomolecular Engineering, University of Tennessee, Knoxville, Tennessee 37996, USA

⁷Computation-based Science and Technology Research Center, The Cyprus Institute, Nicosia 2121, Cyprus

⁸Department of Mathematics and Applied Mathematics, University of Crete, Heraklion GR-71110, Greece



(Received 9 December 2022; revised 13 September 2023; accepted 29 February 2024; published 13 May 2024)

Through the analysis of the spatial correlations of local stress, we detect the propagation of long-ranged liquid-elasticity-mediated shear stress waves in polymeric and low-molecular weight liquids. The propagation of shear waves is effectively planar; i.e., $\sigma_{\alpha\beta}$ propagates in the $\alpha\beta$ plane. The autocorrelation functions of the local stress of a region are affected by both the relaxation of stress in that region and the propagation of stress from the region to the rest of the sample. However, due to the planar propagation of shear waves, the transfer of $\sigma_{\alpha\beta}$ from those slices of the simulation box that are periodic in the $\alpha\beta$ plane is negligible. This allows direct probing of the position-dependent local stress relaxation modulus of liquid in the vicinity of a confining surface.

DOI: [10.1103/PhysRevResearch.6.023161](https://doi.org/10.1103/PhysRevResearch.6.023161)

I. INTRODUCTION

Calculating the local viscoelastic properties of liquids in the vicinity of interfaces is the key to understanding the rheological behavior of a range of emerging materials such as polymer nanocomposites, thin polymer films, and nanoconfined liquids. Experimentally, efforts have been made to measure some local rheological properties in inhomogeneous systems employing techniques such as x-ray photon correlation spectroscopy [1] and atomic force microscopy [2–4].

Concerning the calculation of viscoelastic properties in simulations, the fluctuation-dissipation theorem connects the autocorrelation function of the total stress of a liquid to its shear stress relaxation modulus, $G(t)$, the basic quantity of linear rheology:

$$G(t) = \frac{V}{k_B T} \langle \sigma_{\alpha\beta}(t) \sigma_{\alpha\beta}(0) \rangle, \quad \alpha \neq \beta. \quad (1)$$

Here V , k_B , T , and $\sigma_{\alpha\beta}(t)$ are the volume, Boltzmann constant, temperature, and an off-diagonal component

($\alpha, \beta \in \{x, y, z\}$) of the instantaneous stress tensor. This relation has been widely used for calculating $G(t)$ in simulations [5–7]. However, its generalization for the calculation of local $G(t)$ [i.e., the $G(t)$ of a specific region of the sample] is not clear, even for single-component liquids, because of possible spatial correlations between the stresses of different parts of the material. Spatially long-ranged stress correlations have been previously observed in different model liquids, and they are usually discussed in terms of the elasticity-induced coupling of local stresses [8–13]. The analysis of spatial correlations of local stress can also be useful for understating the mechanism of the structural relaxation of the supercooled liquids [8,14,15].

Few works have discussed the generalization of Eq. (1) for the calculation of local $G(t)$. Levashov *et al.* [16] analyzed the correlation between the stress of an atom of a liquid and the stress of a group of atoms located in a spherical shell around that atom. Through this analysis, they detected the propagation of stress waves in the liquid and concluded that viscosity [which is the integral of Eq. (1)] is highly nonlocal, and its relevant lengthscale is the range of shear-wave propagation. According to their conclusion, Eq. (1) cannot be used to calculate the local viscosity of a region if the region is smaller than the lengthscale of wave propagation, which can be very large. More recently [17], it was suggested, although without an analysis of the spatial correlations of local stress, to calculate the correlation between the local stress of a region and the total stress for the calculation of local $G(t)$.

*aforooza@uni-mainz.de

†petra.bacova@uca.es

‡v.harmandaris@cyi.ac.ye

Published by the American Physical Society under the terms of the [Creative Commons Attribution 4.0 International](https://creativecommons.org/licenses/by/4.0/) license. Further distribution of this work must maintain attribution to the author(s) and the published article's title, journal citation, and DOI.

In this work, we focus on the study of the spatiotemporal correlations of local stresses of subregions of bulk and confined polymeric and low-molecular weight liquids with the main goals of (i) investigating the applicability of Eq. (1) for the calculation of the $G(t)$ of a given region of material, and (ii) probing spatially resolved (at the nanoscale) signals about stress relaxation in a nanoconfined system. Because of their pronounced viscoelastic behavior and their practical importance, we focus on polymeric liquids. Specifically, we report results of equilibrium atomistic molecular-dynamics simulations of melt of unentangled *cis*-1,4-polybutadiene (cPB) chains. We start by examining the homogeneous bulk cPB melt and then extend the investigation to the melt confined between periodic amorphous silica (SiO₂) surfaces. Moreover, to investigate the generality of our findings, we analyze generic coarse-grained liquids of different molecular weights, namely 1, 30, or 100 beads per chain, using a standard bead-spring model [18].

II. MODEL AND METHOD

Simulations were carried out using the LAMMPS package [19]. In all cases, periodic boundary conditions were applied in all directions.

A. Atomistic simulations

A validated united atom model [20–22] was used for the simulation of *cis*-1,4-polybutadiene (cPB) chains, each containing 30 monomers, corresponding to 120 united atoms. Simulations were carried out in the *NVT* ensemble, using the Nosé-Hoover thermostat. The initial well-equilibrated configurations were taken from long-time *NPT* simulations. For the simulation of the bulk melt, the nonbonded interactions were cut off at 1 nm, and van der Waals tail corrections were applied to energy and pressure. A time step of 1 fs was used for the integration of the equations of motion. To investigate system size effects, we simulated three different systems containing 100, 400, and 1600 chains in the box. At $T = 413$ K, which is the temperature at which most simulations were performed, the above numbers of chains resulted to the following box sizes, respectively: $6.74 \times 6.76 \times 6.94$ nm, $6.74 \times 6.76 \times 27.77$ nm, and $6.74 \times 6.76 \times 111.09$ nm along the *xyz* directions.

We also simulated cPB melt confined between silica slabs. The amorphous silica slab contains silicon, oxygen, and hydrogen atoms and was modeled using an all-atom force field [23–25]. A periodic slab was placed in the box parallel to the *xy* plane. The periodic boundary condition along the *z* direction confines the cPB melt between the slab and its periodic image. In the case of the confined melt, nonbonded interactions were truncated at 2 nm and van der Waals tail corrections were not applied. Also, a 1 fs time step was used for the integration of the equations of motion. The confined film contains 261 chains. The dimensions of the slab and the box are shown in Fig. 5.

B. Generic coarse-grained simulations

Coarse-grained simulations were performed using the Kremer-Grest bead-spring model [18]. In this model, the repulsive part of a Lennard-Jones potential describes the non-

bonded interactions between the beads, and a FENE potential describes the bond-stretching interaction in the chains. Simulations were carried out with reduced units ($\sigma = 1$, $\varepsilon = 1$, $m = 1$). The bead-spring models contain 1, 30, or 100 beads per chain. The single-bead system does not have FENE bonds. In all cases, the bead density is equal to $0.85\sigma^{-3}$. The number of molecules in the box is equal to 3000, 100, and 100 for 1-bead, 30-bead, and 100-bead liquids, respectively. Simulations were performed at $T = 1$ using the Langevin thermostat (with a bead friction of $0.5\tau^{-1}$), and $dt = 0.01\tau$ was used for solving the equations of motion.

C. Calculation of local stress

The instantaneous stress of a region at time t is calculated from the per-atom stresses of the atoms present in that region at time t . In the absence of long-range interactions, the different components of the stress tensor of atom i , $\sigma_{i\alpha\beta}$ ($\alpha, \beta \in \{x, y, z\}$), are calculated through [26]

$$\begin{aligned}
 -\sigma_{i\alpha\beta}\mathcal{V}_i = & mv_{i\alpha}v_{i\beta} + \frac{1}{2} \sum_{\text{pairs}} (r_{i\alpha}F_{i\beta}^{\text{pair}} + r_{j\alpha}F_{j\beta}^{\text{pair}}) \\
 & + \frac{1}{2} \sum_{\text{bonds}} (r_{i\alpha}F_{i\beta}^{\text{bond}} + r_{j\alpha}F_{j\beta}^{\text{bond}}) \\
 & + \frac{1}{3} \sum_{\text{angles}} (r_{i\alpha}F_{i\beta}^{\text{ang}} + r_{j\alpha}F_{j\beta}^{\text{ang}} + r_{k\alpha}F_{k\beta}^{\text{ang}}) \\
 & + \frac{1}{4} \sum_{\text{dihedrals}} (r_{i\alpha}F_{i\beta}^{\text{dihed}} + r_{j\alpha}F_{j\beta}^{\text{dihed}} \\
 & \quad + r_{k\alpha}F_{k\beta}^{\text{dihed}} + r_{l\alpha}F_{l\beta}^{\text{dihed}}), \quad (2)
 \end{aligned}$$

where \mathcal{V} , \vec{v} , \vec{r} , and \vec{F} label the volume of the atom, the velocity, the position, and the force, respectively. Indices j , k , and l represent different atoms. Atomic volume \mathcal{V}_i is on the left-hand side of the above equation, as it is generally difficult to assign to a particular atom. The first term on the right-hand side of Eq. (2) is the kinetic energy contribution to the atomic stress, the second term is the pairwise nonbonded energy contribution, and the sum is taken over all neighbors of the atom i that have nonbonded interactions with it. The third, fourth, and fifth terms account for the contribution of bond, angle, and dihedral interactions; here, the sums are taken over all bonds, angles, and dihedral angles that the atom i participates in. A virial contribution that is produced by bonded and nonbonded interactions using the aforementioned terms between two, three, and four atoms is shared in equal portions between these atoms [consider factors 1/2, 1/3, and 1/4 in Eq. (2)].

To calculate the stress of a region, $\sigma_{\text{reg}}(t) = [\sum_i \sigma_i(t)\mathcal{V}_i]/V_{\text{reg}}$ is used; here, the sum runs over all atoms i that are present in the region at the time t , and V_{reg} is the volume of this region. In the case of partitioning the simulation box into some regions, $\sigma(t) = \sum \phi_i \sigma_i(t)$, where $\sigma(t)$ is the instantaneous total stress of the systems, and σ_i and ϕ_i are the stress and the volume fraction of the region i .

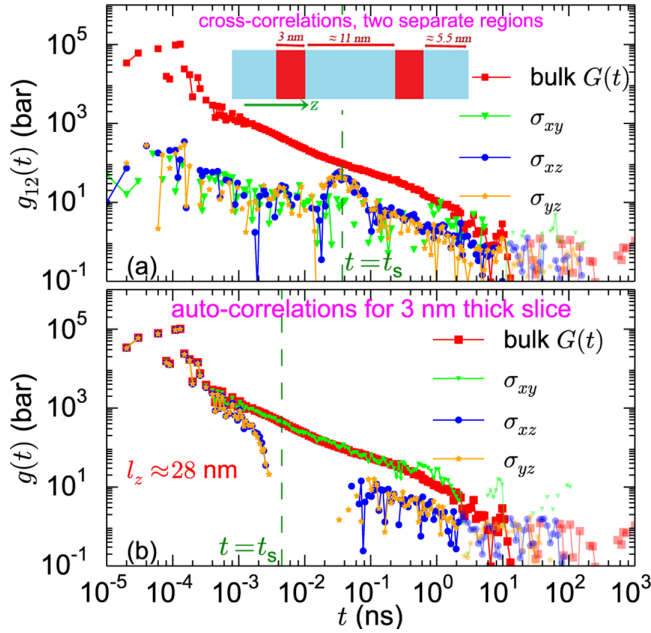


FIG. 1. (a) The cross-correlations between the local stresses of two 3-nm-thick slices of the simulation box. The minimum distance between the slices is 11 nm. (b) The autocorrelation of the local stress of one of the slices. The vertical dashed line corresponds to the estimated timescale of shear stress transfer between the regions. To improve visibility, the long-time noisy data are semi-transparent ($T = 413$ K).

III. RESULTS AND DISCUSSION

To investigate the spatiotemporal correlations of the stresses of different parts of the material, we analyze the autocorrelation of the local stress of a given region, $g(t)$, or the cross-correlation between the stresses of two different regions, $g_{ij}(t)$, defined as

$$g(t) = \frac{V_i}{k_B T} \langle \sigma_i(t) \sigma_i(0) \rangle, \quad g_{ij}(t) = \frac{V_j}{k_B T} \langle \sigma_j(t) \sigma_i(0) \rangle. \quad (3)$$

Here i and j are the indices of the regions. The correlation functions were calculated using the multiple-tau correlator algorithm [27].

A. Bulk liquids

Figure 1(a) shows $g_{12}(t)$, the cross-correlations between the stress of two slices of the simulation box (of cPB melt) which are 3 nm thick and lie 11 nm far apart from each other along the z direction ($T = 413$ K). The slices are periodic in the x and y directions [see the inset of Fig. 1(a)]. The average radius of gyration of the cPB chains, R_g , equals 1.44 nm. Here, the dimensions of the simulation box are about $7 \times 7 \times 28$ nm³ along the xyz directions, respectively. In this geometry, the distance between a slice and the periodic image of the other slice is also ≈ 11 nm, and hence $g_{12}(t)$ contains the contribution from the stress transfer to the periodic image. The $G(t)$ of the bulk cPB is also shown in Fig. 1. The $g_{12}(t)$ for the xy component fluctuates between positive and negative values up to the terminal time (final decay) of the bulk $G(t)$ (negative values are not shown in the logarithmic scale).

This behavior suggests that the correlation between σ_{xy} of the two regions is insignificant. The situation is different for σ_{xz} and σ_{yz} . At intermediate times, the cross-correlations of these components show a clear peak. This peak is a direct sign of the transfer of σ_{xz} and σ_{yz} between the two considered regions. Note that the peak time of the $g_{12}(t)$ [≈ 0.03 ns in Fig. 1(a)] is around three orders of magnitude smaller than the timescale of the translation of chains from one region to the other [at the terminal time of $G(t)$, around 3 ns in Fig. 1, a chain displaces on average a distance comparable to its size, R_g].

Stress is transferred between different regions through the propagation of stress waves. A local rearrangement of the particles (a local relaxation event) sets up a local deformation in the liquid. This local deformation leads to an elastic deformation in the surrounding liquid, which at short times behaves like an elastic medium [8,15]. Because of the short-time elasticity of liquid, this elastic deformation propagates in the liquid, before its dissipation by the relaxation processes. Following the above picture, stress is transferred between two regions when the stress waves originating in one region arrive at the other one. Also, at short times, smaller than the characteristic time of the wave transfer, stress transfer is negligible, consistent with the short-time behavior of the cross-correlations of σ_{xz} and σ_{yz} in Fig. 1(a) (which at short times have large positive and negative fluctuations). Based on the elasticity-mediated wave propagation picture, we can also estimate a timescale for the transfer of stress between two regions using $t_s = d/v$, where v is the speed of the stress waves and d is the lengthscale of the wave motion. The speed of shear-stress waves in an elastic material equals $\sqrt{G/\rho}$, where G and ρ are the shear modulus and density. For estimating the speed of shear waves in the liquids, we use $v = \sqrt{G_0/\rho}$, where G_0 is the short time value of $G(t)$ before the structural (segmental) relaxation time (timescales in which the material behaves elastically). At $T = 413$ K the value of $G(t)$ at 1.5 ps is used for the estimation of the velocity of shear waves. In the case of the atomistic cPB model, this time is right after the regime of bond and angle oscillations [which are seen in bulk $G(t)$ at subpicosecond timescales]. The estimated velocity is $v = 334$ m/s. To estimate the average distance that a wave needs to travel between two regions, we assume a source of stress wave in the middle of a region and calculate the distance between the source and the other region. So, for the lengthscale of wave motion, we estimate $d = 12.5$ nm for the geometry of Fig. 1(a). Interestingly, the calculated timescales of stress transfer, t_s , which is shown in Fig. 1(a) by a vertical dashed line, (almost) corresponds to the peak time of the cross-correlations of σ_{xz} and σ_{yz} . The agreement between the calculated t_s value and the peak times of $g_{12}(t)$ is a confirmation for the wave-propagation picture that underlies the calculations. Before their dissipation, shear waves can have a lifetime of the order of the terminal time of $G(t)$. The terminal time and therefore the lengthscale of wave motion (or the lengthscale of local-stress correlations) increases upon reducing temperature or, in the case of polymer melts, upon increasing chain length.

The insignificant transfer of σ_{xy} between the different regions discussed above is a clear indication that the propagation of the shear stress waves is not isotropic. Based on this observation, the propagation of σ_{xy} should mainly

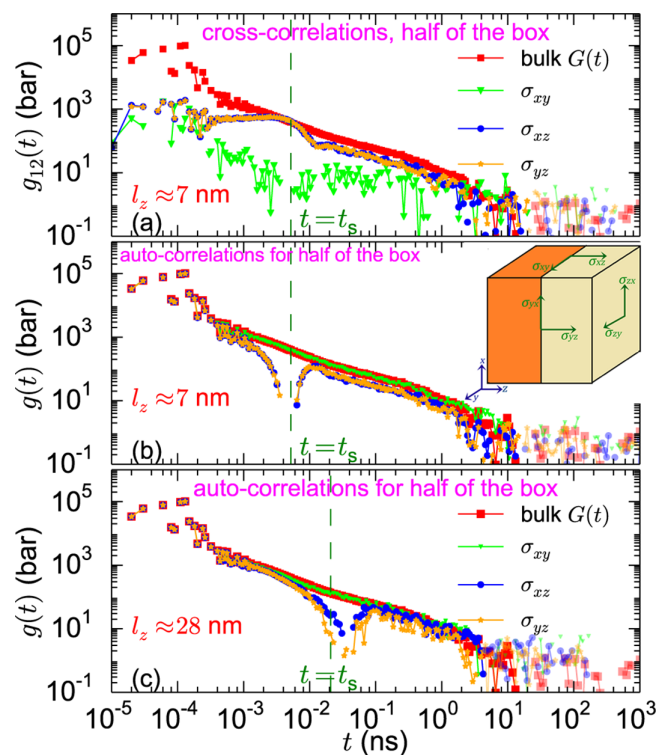


FIG. 2. (a) The cross-correlation between the local stresses of the two halves of the simulation box [see the inset of panel (b)]. Panels (b) and (c) show the autocorrelation of different stress components of one-half of the box; $l_z \approx 7$ nm in panels (a) and (b) and $l_z \approx 28$ nm in panel (c).

occurs on the xy plane, and the propagation along the z direction should be negligible. This is in agreement with the development of 2D-like shear stress correlations in the inherent structures of a 3D liquid, as observed previously [10] and also with the results presented in Fig. 1(b), as discussed below.

Figure 1(b) shows the $g(t)$ curves, autocorrelations of different stress components of one of the 3-nm-thick slices shown in panel (a). The $g(t)$ of the xy component is almost identical to the bulk $G(t)$, while the $g(t)$ of the xz and yz components differ significantly from the bulk behavior. The propagation of σ_{xy} along the z direction is negligible, hence the decay of the $g(t)$ of σ_{xy} originates from the relaxation of stress in the region and is similar to the bulk relaxation curve. On the contrary, σ_{xz} and σ_{yz} propagate from the considered region to the rest of the system; hence, the decay of their $g(t)$ does not merely stem from the relaxation of the stress in the region, but it is also affected by the stress transfer to the rest of the box. So, the $g(t)$ of these components differs from the bulk $G(t)$. The timescale of stress transfer from the slice to the rest of the box, shown in panel (b) and estimated using $d = 1.5$ nm for the lengthscale of wave motion, almost corresponds to the time of the large drop in the $g(t)$ of σ_{xz} and σ_{yz} .

Next, we investigate the stress transfer between two adjacent regions. For this, we divide the simulation box, along the z axis, into two slices of the same size which are periodic along two directions [see the inset of Fig. 2(b)]. Figure 2(a) shows the cross-correlations between the stresses of the first

and the second regions, and Fig. 2(b) shows the $g(t)$ for different stress components of one of the regions, i.e., half of the box. The results presented in panels (a) and (b) have been calculated using a box with dimensions approximately equal to $7 \times 7 \times 7$ nm³. Consistent with the results of Fig. 1, σ_{xz} and σ_{yz} are transferred between the two halves of the simulation box; this is reflected in the large values of their cross-correlation functions [see Fig. 2(a)] and leads to the deviation of their $g(t)$ from the bulk $G(t)$. For the xy component, $g(t)$ is similar to the bulk relaxation curve [see Fig. 2(b)] because stress transfer between the regions is negligible [$g_{12}(t)$ exhibits large positive and negative fluctuations].

To examine system size effects, in Fig. 2(c) we present the $g(t)$ curves for half of the box, however with l_z being four times larger than that in panels (a) and (b). For the $g(t)$ of σ_{xz} and σ_{yz} , the onset of deviation from the bulk $G(t)$ shifts to longer times with increasing l_z . With increasing the thickness of the adjacent regions (i.e., increasing l_z), the stress waves originating from a region need to travel a longer distance before arriving at the other region, hence the time of stress transfer is higher. The timescales of stress transfer, estimated using $d = l_z/4$ for the lengthscale of wave motion, are shown in Fig. 2. They are in line with the time of the large drop in the $g(t)$ of σ_{xz} and σ_{yz} components, and also with the time at which their cross-correlations reach a local maximum in Fig. 2(b). Based on the above discussion, if the time of stress transfer is longer than the terminal time of $G(t)$, most of the stress waves are dissipated before traveling between the regions, and the deviation of the $g(t)$ of all stress components from the bulk $G(t)$ becomes negligible. We have also simulated cPB melt with an even larger box size ($l_z \approx 111$ nm) (Fig. 9 of Appendix A), and cPB melt at a lower temperature of 253 K at which a plateau-like glassy regime is seen in the $G(t)$ curve (Fig. 10). In these cases, the results are consistent with trends presented in Fig. 2. A brief discussion about the relaxation of normal stress fluctuations is also provided in Appendix A 3.

Next, we present the results for the coarse-grained bead-spring liquids. Figure 3 shows the cross-correlations, $g_{12}(t)$, and autocorrelations, $g(t)$, for the case of dividing the simulation box, along the z axis, into two equally sized regions (the geometry shown in Fig. 2); the panels of Fig. 3 show the results for single-bead (Lennard-Jones liquid), 30-bead, and 100-bead systems. In each case, the total $G(t)$ of the liquid is also presented. The Lennard-Jones liquid does not have any bonds; hence, the short-time bond oscillation regime is not observed in its $G(t)$. The behavior of $g_{12}(t)$ and $g(t)$ for the coarse-grained models is consistent with the results for the cPB melt shown in Fig. 2. For all coarse-grained liquids, the $g_{12}(t)$ of σ_{xy} is significantly smaller than $g_{12}(t)$ of σ_{xz} and σ_{yz} . Furthermore, the $g(t)$ of σ_{xy} is similar to the bulk $G(t)$, whereas the $g(t)$ of the xz and yz stress components is different from the bulk $G(t)$. These results are consistent with the propagation of σ_{xz} and σ_{yz} along the z axis from one-half of the simulation box to the other one.

We also estimated the speed of shear stress waves in these liquids from the short-time value of $G(t)$ using $\sqrt{G_0/\rho}$. The estimated values of shear wave velocity are $6.63\sigma/\tau$, $8.75\sigma/\tau$, and $9.04\sigma/\tau$ for the liquids containing 1-bead, 30-bead- and 100-bead molecules, respectively. These velocities were calculated from the value of $G(t)$ at $10^{-2}\tau$ around which

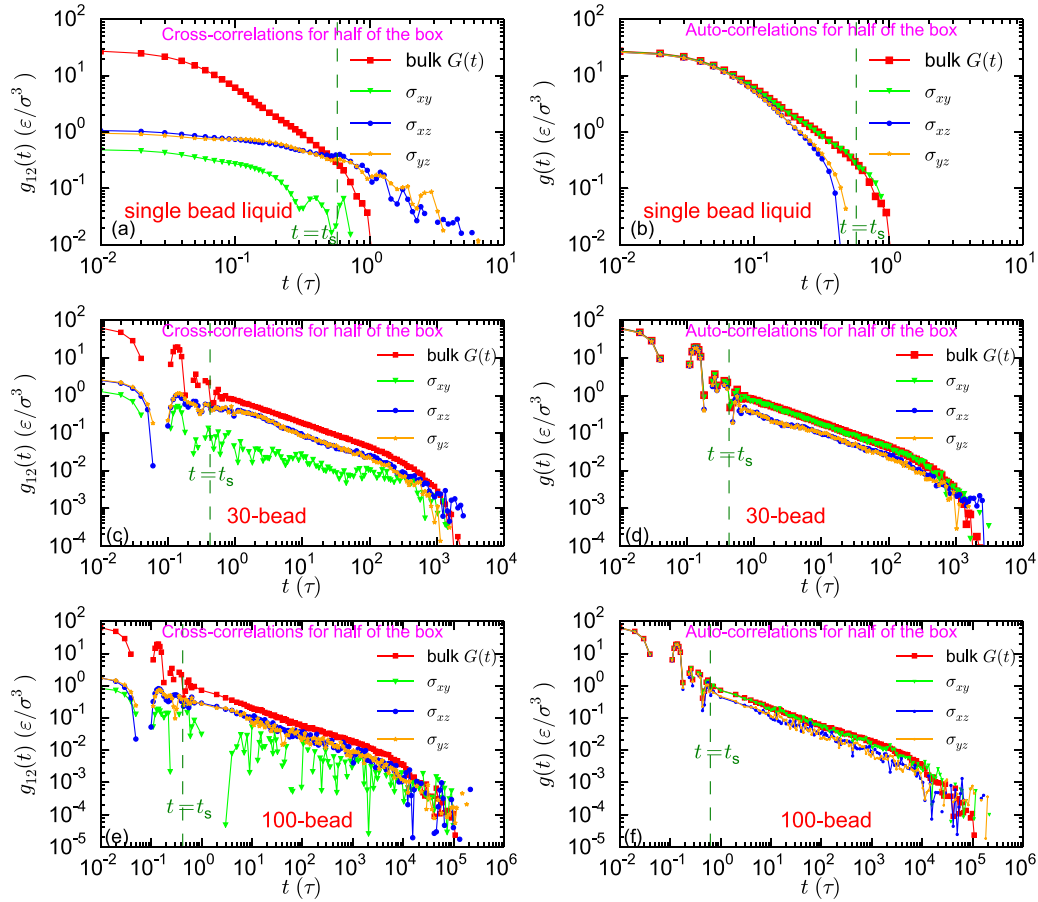


FIG. 3. The results for the generic coarse-grained model liquids. Panels (a), (c), and (e) show the cross-correlation functions between the local stresses of the first and the second region of the simulation box, for 1-bead, 30-bead, and 100-bead systems, respectively. Panels (b), (d), and (f) show the autocorrelation functions of different stress components of half of the box, for 1-bead, 30-bead, and 100-bead systems, respectively.

$G(t)$ shows its glassy regime. Note that, for 30-bead and 100-bead chains, this timescale is smaller than the timescale of bond oscillations. In this coarse-grained model, the bonds are rather soft, and the timescale of their oscillation is long. We have observed such behavior for other coarse-grained models [6].

The estimated timescale of stress transfer (using $l_z/4$ for the timescale of wave motion, as discussed above) is shown with vertical dashed lines in Fig. 3. For a 1-bead system, the time of the stress transfer almost corresponds to the time of the large drop in the $g(t)$ of σ_{xz} and σ_{yz} . For 30-bead and 100-bead systems, stress transfer coincided with the bond-oscillation regime; hence, the deviation of local $g(t)$ from the bulk $G(t)$ happens after the bond-oscillation regime.

To elaborate further on the behavior of $g(t)$, we investigate the domain size effect. We calculate the autocorrelations of σ_{xy} coming from the slices of different thicknesses. The slices extend periodically in the xy plane. As Fig. 4(a) shows, for the cPB melt, the $g(t)$ curves (of σ_{xy}) for the slices with thicknesses of 3.5 and 2 nm closely follow the bulk $G(t)$. However, for thin 1 and 0.5 nm slices, the $g(t)$ curves are systematically below it. Panels (b), (c), and (d) of Fig. 4 show the effect of the layer thickness for single-bead, 30-bead, and 100-bead liquids, respectively. The van der Waals radius of the coarse-grained beads equals 1.26σ , and the radii of

gyration of the 30-bead and 100-bead chains equal 2.8σ and 5.27σ , respectively. For all model liquids, the $g(t)$ for the layers with a thickness of 1σ is significantly below the bulk $G(t)$. However, by increasing the layer thickness, $g(t)$ tends to the bulk $G(t)$. The results suggest that R_g is not the relevant lengthscale for the layer-thickness dependence of the $g(t)$ of σ_{xy} . Rather, it seems that at lengthscales larger than a few particle (bead) sizes (possibly corresponding to the lengthscale of local particle rearrangements in the liquid), the local $g(t)$ of σ_{xy} converges to the bulk $G(t)$. This is also in agreement with the result of the atomistic simulations as the van der Waals radius of the united atoms of the model cPB chains is around 0.42 nm.

B. Confined polymer melt

After examining the homogeneous melt, we consider the cPB melt embedded between periodic amorphous silica slabs. In this section, our main goal is the calculation of the position-dependent local stress relaxation modulus of the melt in the vicinity of the solid surface. Figure 5(a) shows a snapshot of the model interfacial system together with the interfacial density profile of the confined melt. In the vicinity of the surface, the density profile shows oscillations that indicate the interfacial layered structure of the melt. The layered structure

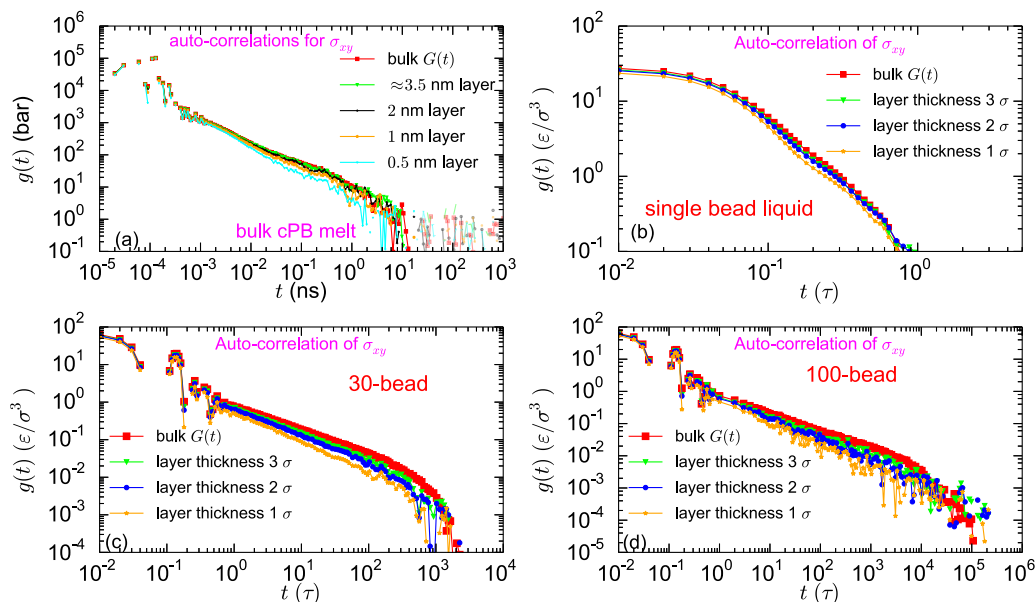


FIG. 4. The effect of the layer thickness on the autocorrelation of σ_{xy} . Panels (a), (b), (c), and (d) show the results for the cPB melt, single-bead, 30-bead, and 100-bead liquids, respectively.

originates from the preferential alignment of the polymer with the surface. Local density oscillations extend up to 2–3 nm from the surface [28]. In systems with effective attractive polymer-surface interactions, polymers physically adsorb on the surface. The adsorbed chains extend up to approximately $R_{ee} = 3.6$ nm from the surface, where R_{ee} is the average end-to-end distance of the chains [see Fig. 5(a)]. However, the adsorbed chains prevail up to distances of around 1.5 nm from the surface. This latter lengthscale almost corresponds to the unperturbed average radius of gyration of the chains ($R_g = 1.44$ nm). Figure 5(b) shows the layer-resolved mean-squared displacements of the monomers, normalized with $t^{0.5}$, in the plane parallel to the confining surface [$MSD_{xy}(t)/t^{0.5}$], as well as the definitions of the various layers. In this presentation, detection of the Rouse scaling regime is easier, as the Rouse model (for long chains) predicts the evolution of

segmental MSD with $t^{0.5}$ before reaching the diffusive regime. The thickness of layer 0 is around 1.5 nm, which almost corresponds to the region where the adsorbed chains are prevailing and also in which local density shows strong oscillations. As also described in detail elsewhere [28], the surface-induced heterogeneity in the mobility of the particles, particularly pronounced in layer 0, originates from the friction imposed by the amorphous and nano-rough surface of the silica slab on the movement of the particles in the parallel direction.

Having identified the lengthscale linked to the distinct dynamical behavior and defined the corresponding layers in the system [see Fig. 5(b)], in what follows we calculate the correlations of local stress in and between these layers. For measuring the stress of a layer, we summed over the contributions of the polymer atoms in that layer. It should be noted that we measured the correlation functions of the fluctuation of

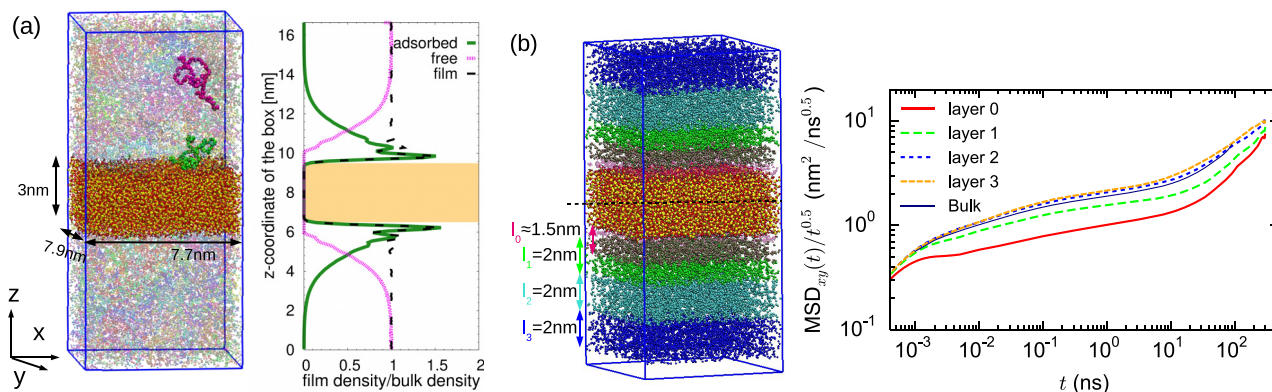


FIG. 5. (a) A snapshot of the model cPB/silica interfacial system, together with the mass density profile of the polymer. The density profiles of adsorbed and free chains are also shown, with the same color scheme as their examples in the snapshots. An atom is assumed to be adsorbed if it is located from the surface at a distance smaller than the first minimum in the density profile. The chains that do not have adsorbed atoms are called free chains. (b) The layer-resolved lateral monomeric mean-squared displacements, normalized with the Rouse slope, $t^{0.5}$. The definitions of the layers are also shown.

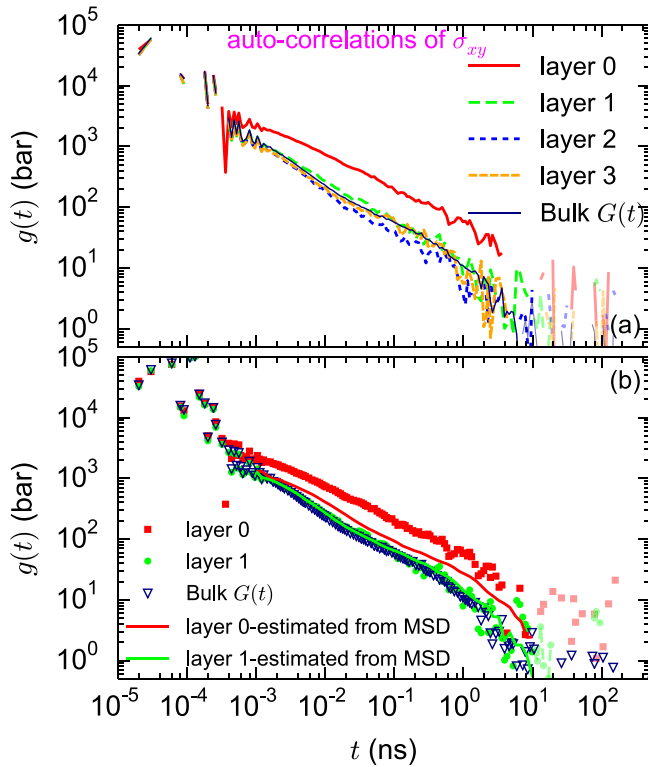


FIG. 6. (a) $g(t)$ of σ_{xy} calculated in different layers of the interfacial system. The long-time noisy data are transparent. (b) $g(t)$ of layers 0 and 1 [data from (a) are plotted with points] compared to the same quantities estimated by using their $\text{MSD}_{xy}(t)$ at $T = 413$ K (lines).

the local shear stress, $\sigma_{\alpha\beta}(t) - \langle \sigma_{\alpha\beta}(t) \rangle$, to remove the effects of any possible residual stresses. The correlation functions of the actual values and of the fluctuations are almost identical, therefore we keep the same notation, but as this might not be the case in some systems, we report the details for completeness.

Figure 6(a) shows the layer-resolved autocorrelation functions of σ_{xy} in the hybrid system. As learned from the analysis of the bulk melt, σ_{xy} propagates in the xy plane, and therefore the transfer of this stress component between layers is negligible. Consistent with negligible stress transfer along the z direction, the local $g(t)$ for the layers far from the slab is similar to the bulk $G(t)$ within the precision obtained. Relaxation of the local stress in layer 0 is slower than in the remaining layers. The deviation from the bulk behavior starts right after the bond and angle vibrations at the timescales corresponding to the segmental dynamics. This is a piece of direct evidence for the effect of the surface on the local stress relaxation modulus of the polymer melt.

The trend observed for the local $g(t)$ is qualitatively consistent with that for the monomer lateral displacements, as presented in Fig. 5(b). The results show that the irregular surface of the amorphous silica imposes effective friction on the translation of segments in the direction parallel to the slab, leading to their slower lateral dynamics, and hence their slower stress relaxation, compared to the bulk system.

To make a quantitative comparison between the behavior of $g(t)$ of σ_{xy} and $\text{MSD}_{xy}(t)$ in the vicinity of the surface, we calculate time-dependent scaling factors to convert bulk MSD to MSD of the layers; then the scaling factors obtained are used to estimate $g(t)$ of the layers from bulk $G(t)$ and then the estimated $g(t)$ functions are compared with the $g(t)$ data measured directly from the stress correlation. Following Borodin *et al.* [29], a time scaling factor, $a(t)$, is defined via $\text{MSD}_{xy}^{\text{layer}}(t) = \text{MSD}_{xy}^{\text{bulk}}[a(t)t]$. Then $g(t)$ is estimated using $G^{\text{bulk}}[a(t)t]$. The estimated $g(t)$ curves for layers 0 and 1 are shown in Fig. 6(b). For layer 0, the estimated $g(t)$ significantly underestimates the measured $g(t)$. Alternatively, another scaling factor can be defined using $z(t) = \text{MSD}_{xy}^{\text{bulk}}(t)/\text{MSD}_{xy}^{\text{layer}}(t)$, and $g(t)$ can be estimated using $z(t)G^{\text{bulk}}(t)$. The results of this procedure are almost similar to the data shown in Fig. 6(b) [calculated using the $a(t)$ defined above]. $z(t)$ can be seen as the ratio of the effective friction felt by the bulk monomers to the friction felt by the monomers in the given interfacial layer, quantified using MSD. At intermediate times, $z(t)$ of layer 0 is around 1.8, however the effect of the surface on the stress relaxation modulus of layer 0 is stronger and, at intermediate times, it is approximately 3.9 times greater than the bulk $G(t)$.

The analysis of stress transfer in the hybrid system is presented in Fig. 7. Figure 7(a) shows the cross-correlations between the stress of the entire confined PB melt and the stress of the silica slab. The cross-correlations of σ_{xz} and σ_{yz} are significant, which shows that, in addition to the propagation of stress in the melt, stress is transferred between the melt and the slab. The cross-correlation of σ_{xy} is much smaller (it fluctuates between positive and negative values), which is consistent with the planar propagation of σ_{xy} in the xy plane. In Fig. 7(b), we investigate the $g(t)$ of the xz stress component, which propagates in the xz plane and hence travels between the layers of the interfacial system along the z direction (data for σ_{yz} are similar). Similar to the bulk behavior, the $g(t)$ functions become negative at intermediate timescales. We link the timescale of this drop with the characteristic time of shear-wave propagation [vertical dashed line in Fig. 7(b)] calculated using $d = 1$ nm (almost half of the thickness of the layers; see Fig. 5) for the lengthscale of the wave motion. Figure 7(c) shows the cross-correlations between the stresses of layers 1 and 2, $g_{12}(t)$. The results are consistent with the trends observed for the bulk melt. The cross-correlation of σ_{xy} is much smaller than the cross-correlations of σ_{xz} and σ_{yz} , because σ_{xy} propagates in the xy plane. The estimated timescale of stress transfer $t_s^{1,2}$ is also shown and almost corresponds to a local maximum of the cross-correlations of σ_{xz} and σ_{yz} . Figure 7(d) shows the cross-correlations between the stresses of layers 1 and 3, $g_{13}(t)$. Layers 1 and 3 are not connected to each other, and the stress waves originating from layer 1 need to pass through layer 2 before reaching layer 3. $t_s^{1,3}$, the timescale of stress transfer between regions 1 and 3, calculated using $d = 3$ nm for the lengthscale of wave motion, almost corresponds to the position of the pronounced maximum of $g_{13}(t)$ of σ_{xz} and σ_{yz} .

As mentioned in Sec. II, upon partitioning the simulation box into some regions, the total stress of the system is equal to the linear combination of the stresses of the regions:

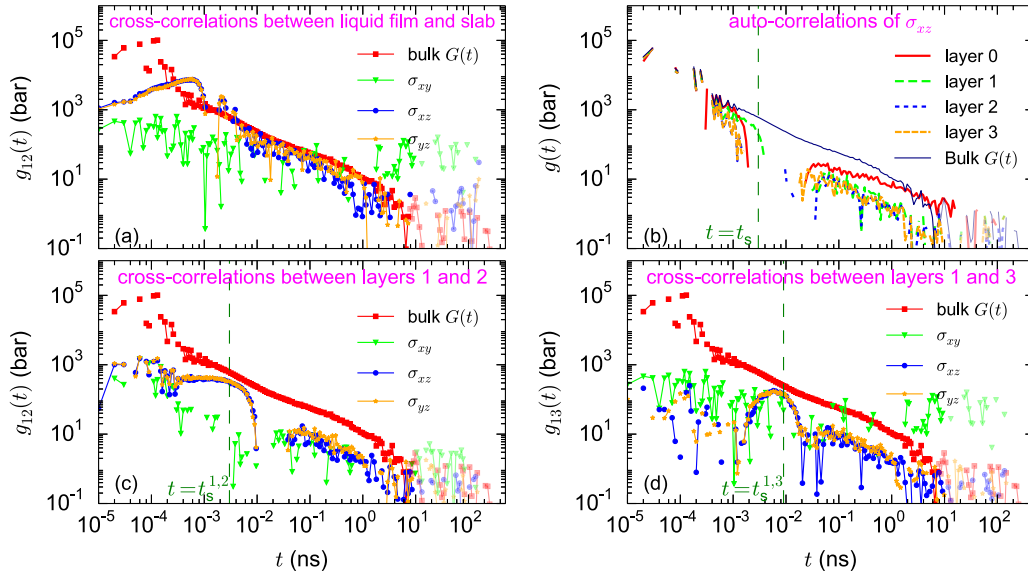


FIG. 7. (a) The cross-correlation between the stress of the confined melt and the stress of the silica slab. (b) $g(t)$ of the σ_{xz} calculated in different layers in the hybrid PB/silica system. (c) The cross-correlation between layers 1 and 2. (d) The cross-correlation between layers 1 and 3. The vertical dashed lines correspond to the estimated times of stress transfer between the regions.

$\sigma(t) = \sum \phi_i \sigma_i(t)$. Inserting this relation into Eq. (1) leads to $G(t) = \sum \phi_i g_{i,\text{total}}(t)$ with $g_{i,\text{total}}(t) = V/k_B T \langle \sigma(t) \sigma_i(0) \rangle$, where $\sigma(t)$ is the total stress of the system at time t and $\sigma_i(0)$ is the local stress of the region i at $t = 0$. Because of the linear form of this relation, one might assume that $g_{i,\text{total}}(t)$ provides a proper description of the stress relaxation in the region, irrespective of stress transfer from the region to the rest of the sample. In other words, one might assume that we can take into account the effect of stress transfer by analyzing the correlation between the stress of a region and the total stress of the system. Figure 8 shows the correlation between σ_{xz} of different layers of the interfacial system and the total σ_{xz} of the system. The total stress includes the stress in the given layer and the stress coming from the remaining polymer and the slab. σ_{xz} propagates in the xz plane and hence is transferred from a layer to the rest of the sample, along the z direction. The layer-resolved correlation curves exhibit oscillations, particularly the curves of layers 0 and 1. This behavior indicates

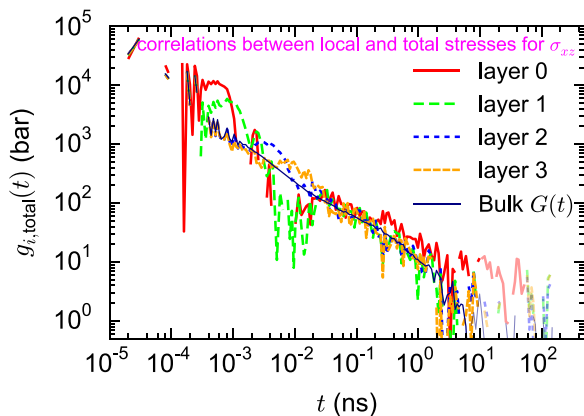


FIG. 8. The correlation between the local σ_{xz} of the layers with the total σ_{xz} of the interfacial system ($T = 413$ K).

that this correlation function is affected by the stress transfer between regions. This is also the case for the correlation of the local stress of a layer and the total stress of polymer film (without the solid slab); see Fig. 12.

IV. SUMMARY

In summary, we performed an analysis of the spatiotemporal correlations of local stress in bulk and nanoconfined polymers and low-molecular weight liquids. Through this analysis, we detected the planar propagation of elasticity-mediated shear stress waves in these systems. Generally, the propagation of stress waves affects the autocorrelation functions of the local stress of a given region of the liquid. However, for the slices of the simulation box that are periodic in the shear wave plane, the propagation of stress to the rest of the sample is negligible, and the autocorrelation of the local stress corresponds to the local stress relaxation modulus. We were able to directly probe the position-dependent local stress relaxation modulus of the polymer melt in the vicinity of a confining surface. The possibility of measuring the spatially resolved stress relaxation modulus is important for understanding the behavior of interfacial systems such as polymer nanocomposites and thin films.

ACKNOWLEDGMENTS

The authors gratefully acknowledge Bing Jiang and Marcus Müller for stimulating discussions. Anthony Chazirakis is also gratefully acknowledged for his help with the LAMMPS package. This work was supported by the computational time granted from the HPC system of the Cyprus Institute (Cyclone), and by the Goodyear Tire & Rubber Company. This work was partially supported by European Unions Horizon 2020 research and innovation program (Grant Agreement No. 810660, SimEA).

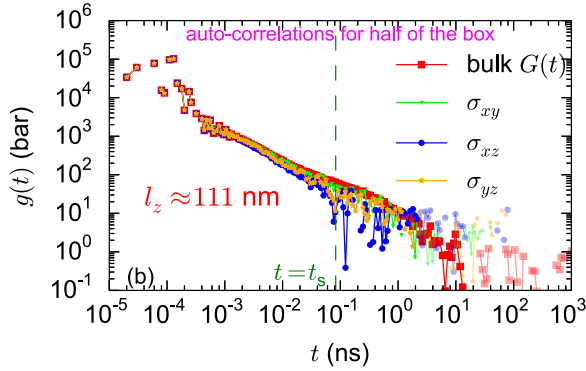


FIG. 9. The autocorrelation of different stress components of one-half of the simulation box; $l_z \approx 111$ nm.

APPENDIX A: SUPPLEMENTAL ANALYSIS OF THE BULK POLYMER MELT

1. Box size effect

Figure 9 shows the autocorrelations of the stress components of half of the simulation box (geometry shown in Fig. 2) for the case of $l_z \approx 111$ nm. Similar to the results presented in Fig. 2, the $g(t)$ of σ_{xz} and σ_{yz} deviate from the bulk $G(t)$ because of the stress transfer between the regions of the box. The estimated timescale of the stress transfer is shown with a dashed vertical line. Because of the large value of l_z , the stress waves originating from one-half of the box stay in that half for a rather long time, and hence the deviation of the $g(t)$ of σ_{xz} and σ_{yz} from the bulk $G(t)$ appears at long times.

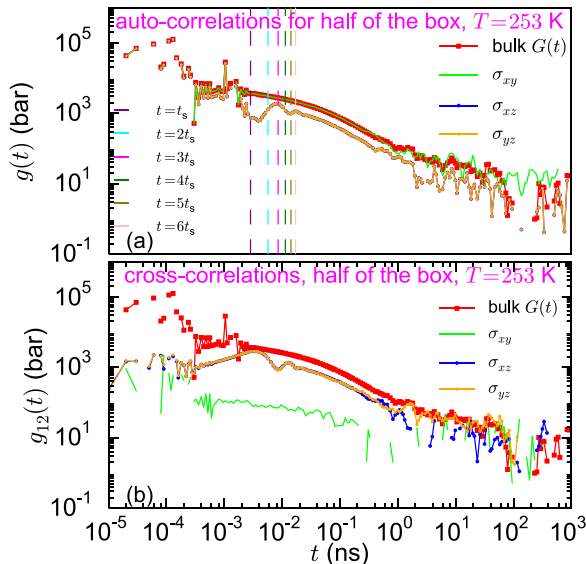


FIG. 10. (a) The autocorrelations of the local stresses of half of the simulation box at $T = 253$ K. (b) The cross-correlations between the stresses of the first and the second region of the simulation box at 253 K. The vertical dashed lines correspond to the multiples of the estimated timescale of the stress transfer between the regions, t_s .

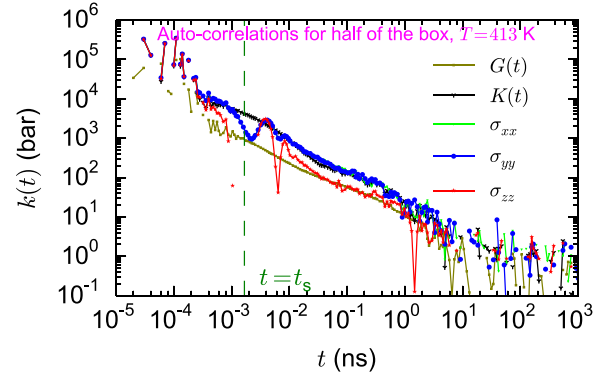


FIG. 11. The autocorrelations [multiplied by $V/(k_B T)$] of different normal (diagonal) components of the local stress tensor collected over half of the simulation box, at $T = 413$ K. The autocorrelations of the global normal [$K(t)$] and shear [$G(t)$] stresses of the polymer in bulk are also provided.

2. Temperature effect

Figure 10 presents the auto- and cross-correlations of the local stresses of half of the box at $T = 253$ K. At $T = 253$ K, the segmental dynamics is well separated from the bond and angle vibrations, and a short-time plateaulike regime representing the glassy behavior can be seen in bulk $G(t)$. The results for $g(t)$ and $g_{12}(t)$ are qualitatively similar to those in bulk at 413 K (Fig. 2). However, the fluctuations observed at intermediate times at 413 K are visible in the auto- and cross-correlation curves of the xz and yz stress components at 253 K as patterns of damped oscillations. To estimate the timescale of the stress transfer between the regions at $T = 253$ K, the value of $G(t)$ at 4 ps, which is smaller than the timescale of the segmental relaxation, is used for the estimation of the velocity of shear waves ($v = 591$ m/s). At this temperature, the speed of shear waves is higher than at 413 K, and therefore the timescale of the stress transfer is lower. The calculated t_s value almost coincides with the maximum of the cross-correlation curve. Some multiples of t_s are also shown in Fig. 10, and they are comparable to the times of the oscillations of auto- and cross-correlation functions.

3. Relaxation of normal stress fluctuations

Here we briefly discuss the autocorrelations of the local normal (diagonal) stress components collected over half of the simulation box, calculated as

$$k(t) = \frac{V}{k_B T} \langle [\sigma_{\alpha\alpha}(t) - \langle \sigma_{\alpha\alpha} \rangle] [\sigma_{\alpha\alpha}(0) - \langle \sigma_{\alpha\alpha} \rangle] \rangle. \quad (\text{A1})$$

$\sigma_{\alpha\alpha}(t)$ is the instantaneous value of a diagonal component of the local stress tensor at time t , and $\langle \sigma_{\alpha\alpha} \rangle$ is the average value of the stress component. Figure 11 shows the autocorrelations of the local normal stresses, the autocorrelation of the total normal stresses of the system, $K(t)$, together with the shear stress relaxation modulus, $G(t)$. Note that $K(t)$ is calculated in an analogous way as $k(t)$ in Eq. (A1), but the diagonal components of the local stress (i.e., the stress of the given region) are replaced by the diagonal components of the global stress (i.e., the stress of the whole system). The

autocorrelation of the local σ_{zz} significantly deviates from the autocorrelation of the global stress in bulk, $K(t)$. For the σ_{xx} and σ_{yy} components, the autocorrelations of the local stresses are close to the autocorrelation of the total stress (excluding the short-time oscillation regime). These results show that σ_{zz} is significantly transferred along the z direction between the two halves of the box.

We also provide an estimate for the timescale of the transfer of normal stresses between the two regions of the box, from the velocity of longitudinal waves. The velocity of longitudinal waves is estimated through $v = \sqrt{K/\rho}$, where K is the compression (bulk) modulus of the melt and ρ is its density. K equals the inverse of the compressibility, and it can be calculated from the fluctuations of the system volume in an *NPT* simulation:

$$\frac{1}{K} = \frac{\langle V^2 \rangle - \langle V \rangle^2}{k_B T \langle V \rangle}. \quad (\text{A2})$$

The timescale of the stress transfer is calculated using $t_s = l_z/4/v$ and shown in Fig. 11 via a dashed vertical line. This estimated timescale coincides with the large (negative) drop of the autocorrelation function of the σ_{zz} stress.

Here, it is worth mentioning that in both cases of shear and normal stresses, the anisotropy of stress propagation in equilibrium has a similarity to the anisotropy of stress transfer under external stresses. Under external stress, the regions that are connected in parallel do not exchange stress, but stress is transferred between the regions connected in series (generally, the regions that are not connected in parallel). In the case of the geometry shown in Fig. 2, the two regions of the box are connected in parallel under σ_{xx} , σ_{yy} , and σ_{xy} stresses (assuming applying external stresses). These stress components directly affect the two regions of the box and the interface between them. Similar to the absence of stress transfer under

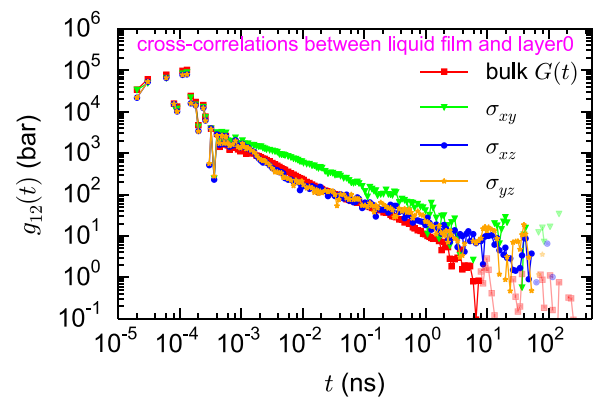


FIG. 12. The correlation between the local stress of layer 0 with the stress of the confined film, without the slab ($T = 413$ K).

external stresses, σ_{xx} , σ_{yy} , and σ_{xy} do not propagate from one region to the other at equilibrium condition. On the contrary, the regions of the box are connected in series under σ_{zz} , σ_{xz} , and σ_{yz} stresses, and these stress components are also transferred between the regions in equilibrium.

APPENDIX B: SUPPLEMENTAL ANALYSIS OF THE INTERFACIAL SYSTEM

Figure 12 shows the correlations between the local stress of layer 0 and the stress of the confined film (without the silica slab), although the stress of the confined liquid is transferred to the solid slab [as shown in Fig. 7(a)]. σ_{xy} does not propagate from the layer to the rest of the sample, and hence the correlation of this component is similar to the autocorrelation of the σ_{xy} of the layer (shown in Fig. 6). The σ_{yz} and σ_{xz} of the layer propagate to the rest of the sample, and the correlations of these stress components are also affected by the stress transfer.

- [1] T. Koga, N. Jiang, P. Gin, M. K. Endoh, S. Narayanan, L. B. Lurio, and S. K. Sinha, Impact of an irreversibly adsorbed layer on local viscosity of nanoconfined polymer melts, *Phys. Rev. Lett.* **107**, 225901 (2011).
- [2] M. Qu, F. Deng, S. M. Kalkhoran, A. Gouldstone, A. Robisson, and K. J. Van Vliet, Nanoscale visualization and multiscale mechanical implications of bound rubber interphases in rubber-carbon black nanocomposites, *Soft Matter* **7**, 1066 (2011).
- [3] H. K. Nguyen, X. Liang, M. Ito, and K. Nakajima, Direct mapping of nanoscale viscoelastic dynamics at nanofiller/polymer interfaces, *Macromolecules* **51**, 6085 (2018).
- [4] D. W. Collinson, R. J. Sheridan, M. J. Palmeri, and L. C. Brinson, Best practices and recommendations for accurate nanomechanical characterization of heterogeneous polymer systems with atomic force microscopy, *Prog. Polym. Sci.* **119**, 101420 (2021).
- [5] A. E. Likhtman, S. K. Sukumaran, and J. Ramirez, Linear viscoelasticity from molecular dynamics simulation of entangled polymers, *Macromolecules* **40**, 6748 (2007).
- [6] A. F. Behbahani, L. Schneider, A. Rissanou, A. Chazirakis, P. Bačová, P. K. Jana, W. Li, M. Doxastakis, P. Polińska, C. Burkhart *et al.*, Dynamics and rheology of polymer melts via hierarchical atomistic, coarse-grained, and slip-spring simulations, *Macromolecules* **54**, 2740 (2021).
- [7] S. Wijesinghe, D. Perahia, T. Ge, K. M. Salerno, and G. S. Grest, Stress relaxation of comb polymer melts, *Tribol. Lett.* **69**, 59 (2021).
- [8] A. Lemaître, Structural relaxation is a scale-free process, *Phys. Rev. Lett.* **113**, 245702 (2014).
- [9] B. Wu, T. Iwashita, and T. Egami, Anisotropic stress correlations in two-dimensional liquids, *Phys. Rev. E* **91**, 032301 (2015).
- [10] S. Chowdhury, S. Abraham, T. Hudson, and P. Harrowell, Long range stress correlations in the inherent structures of liquids at rest, *J. Chem. Phys.* **144**, 124508 (2016).
- [11] M. Hassani, E. M. Zirdehi, K. Kok, P. Schall, M. Fuchs, and F. Varnik, Long-range strain correlations in 3d quiescent glass forming liquids, *Europhys. Lett.* **124**, 18003 (2018).
- [12] L. Klochko, J. Baschnagel, J. Wittmer, and A. Semenov, Long-range stress correlations in viscoelastic and glass-forming fluids, *Soft Matter* **14**, 6835 (2018).
- [13] D. Steffen, L. Schneider, M. Müller, and J. Rottler, Molecular simulations and hydrodynamic theory of nonlocal shear-stress correlations in supercooled fluids, *J. Chem. Phys.* **157**, 064501 (2022).
- [14] M. Maier, A. Zippelius, and M. Fuchs, Emergence of long-ranged stress correlations at the liquid to glass transition, *Phys. Rev. Lett.* **119**, 265701 (2017).

- [15] M. Ozawa and G. Biroli, Elasticity, facilitation, and dynamic heterogeneity in glass-forming liquids, *Phys. Rev. Lett.* **130**, 138201 (2023).
- [16] V. A. Levashov, J. R. Morris, and T. Egami, Viscosity, shear waves, and atomic-level stress-stress correlations, *Phys. Rev. Lett.* **106**, 115703 (2011).
- [17] H. Mori and N. Matubayasi, Local viscoelasticity at resin-metal interface analyzed with spatial-decomposition formula for relaxation modulus, *J. Chem. Phys.* **151**, 114904 (2019).
- [18] K. Kremer and G. S. Grest, Dynamics of entangled linear polymer melts: A molecular-dynamics simulation, *J. Chem. Phys.* **92**, 5057 (1990).
- [19] A. P. Thompson, H. M. Aktulga, R. Berger, D. S. Bolintineanu, W. M. Brown, P. S. Crozier, P. J. in't Veld, A. Kohlmeyer, S. G. Moore, T. D. Nguyen *et al.*, LAMMPS—a flexible simulation tool for particle-based materials modeling at the atomic, meso, and continuum scales, *Comput. Phys. Commun.* **271**, 108171 (2022).
- [20] G. D. Smith and W. Paul, United atom force field for molecular dynamics simulations of 1, 4-polybutadiene based on quantum chemistry calculations on model molecules, *J. Phys. Chem. A* **102**, 1200 (1998).
- [21] G. Smith, W. Paul, M. Monkenbusch, L. Willner, D. Richter, X. Qiu, and M. Ediger, Molecular dynamics of a 1, 4-polybutadiene melt. comparison of experiment and simulation, *Macromolecules* **32**, 8857 (1999).
- [22] A. F. Behbahani, A. Rissanou, G. Kritikos, M. Doxastakis, C. Burkhart, P. Políńska, and V. A. Harmandaris, Conformations and dynamics of polymer chains in cis and trans polybutadiene/silica nanocomposites through atomistic simulations: From the unentangled to the entangled regime, *Macromolecules* **53**, 6173 (2020).
- [23] P. E. Lopes, V. Murashov, M. Tazi, E. Demchuk, and A. D. MacKerell, Development of an empirical force field for silica. Application to the quartz-water interface, *J. Phys. Chem. B* **110**, 2782 (2006).
- [24] T. V. Nodoro, E. Voyiatzis, A. Ghanbari, D. N. Theodorou, M. C. Böhm, and F. Müller-Plathe, Interface of grafted and ungrafted silica nanoparticles with a polystyrene matrix: Atomistic molecular dynamics simulations, *Macromolecules* **44**, 2316 (2011).
- [25] Y. N. Pandey and M. Doxastakis, Detailed atomistic Monte Carlo simulations of a polymer melt on a solid surface and around a nanoparticle, *J. Chem. Phys.* **136**, 094901 (2012).
- [26] A. P. Thompson, S. J. Plimpton, and W. Mattson, General formulation of pressure and stress tensor for arbitrary many-body interaction potentials under periodic boundary conditions, *J. Chem. Phys.* **131**, 154107 (2009).
- [27] J. Ramírez, S. K. Sukumaran, B. Vorselaars, and A. E. Likhtman, Efficient on the fly calculation of time correlation functions in computer simulations, *J. Chem. Phys.* **133**, 154103 (2010).
- [28] P. Bačová, W. Li, A. F. Behbahani, C. Burkhart, P. Políńska, M. Doxastakis, and V. Harmandaris, Coupling between polymer conformations and dynamics near amorphous silica surfaces: A direct insight from atomistic simulations, *Nanomaterials* **11**, 2075 (2021).
- [29] O. Borodin, D. Bedrov, G. D. Smith, J. Nairn, and S. Bardenhagen, Multiscale modeling of viscoelastic properties of polymer nanocomposites, *J. Polym. Sci. Part B* **43**, 1005 (2005).